International Journal of Non-Linear Mechanics 149 (2023) 104310

Contents lists available at ScienceDirect

International Journal of Non-Linear Mechanics

journal homepage: www.elsevier.com/locate/nlm

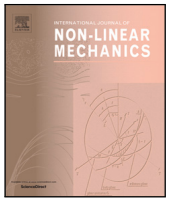

Amplitude–frequency response of parametric resonance of electrostatically actuated MEMS clamped circular plate

Dumitru I. Caruntu *, Reynaldo Oyervides

University of Texas Rio Grande Valley, Mechanical Engineering Department, Edinburg, TX, 78539, USA

ARTICLE INFO

Keywords:
Electrostatically actuated
Frequency–amplitude response
MEMS circular plates
Parametric resonance

ABSTRACT

This paper investigates the amplitude–frequency response of parametric resonance of a clamped elastic circular plate microelectromechanical system (MEMS) resonator above a parallel ground plate and under electrostatic actuation. Soft AC voltage with frequency near the first natural frequency of the plate is used. This results into parametric resonance. The system is assumed to be weakly nonlinear. Numerical and analytical methods are used to solve the reduced order models of the electrostatically actuated MEMS circular plate resonators in order to obtain the amplitude–frequency response of their parametric resonance. Seven Reduced Order Models (ROM) with one to seven modes of vibration (terms) have been developed and used in this investigation. ROM with one mode of vibration was solved using the Method of Multiple Scales (MMS) and predicted the existence of the resonance. ROMs with two to seven modes of vibration were solved using continuation and bifurcation software AUTO 07p to simulate and predict the amplitude–frequency response. These simulations showed that increasing the number of modes of vibration in the ROM produced better results. However, there is no significant difference between six and seven modes of vibration ROMs. Therefore, the ROM using seven modes of vibration was used in this research. This ROM was also numerically integrated to predict time responses of the MEMS plate. All methods showed an excellent agreement for amplitudes less than 0.5 of the gap. Only ROM using seven modes of vibrations had accurate predictions for all amplitudes, i.e. amplitudes between zero and the gap distance. The frequency response consists of two bifurcations, subcritical and supercritical. The effects of AC voltage and damping on the amplitude–frequency response are reported. Increasing the AC voltage results in shifting of the bifurcations to lower frequencies, subcritical significantly more than supercritical. Increasing the damping results in a narrower frequency range between the bifurcations.

1. Introduction

Micro-Electromechanical Systems (MEMS) are attractive for many applications. Such applications include MEMS resonator sensors for measurement of density and viscosity [1–3], voltage detection [4], capacitive detection of large amplitudes of motion [5], and microbalances [6]. Resonator sensors are based on the change of resonance frequency due to the change of environmental properties or mass addition to the system. Capacitive detection is based on the change in distance between plates that causes changes in the capacitance, and can be measured as electrical signal [7].

Electrostatically actuated MEMS are excellent candidates in many applications due to their simple design and accurate control [8]. Such MEMS devices consist of an elastic plate (or beam) held above a parallel rigid ground plate (electrode). When a Direct Current (DC) voltage is applied between the two plates, an electrostatic force causes the elastic plate to deform towards the ground plate. When an Alternating Current (AC) voltage is applied between the two plates, the electrostatic force causes the elastic plate to vibrate. Electrostatic forces and damping forces [9–11] act on the vibrating plate. The vibration of the plate can be controlled by varying the AC voltage and frequency [12]. The electrostatic force is nonlinear being inversely proportional to the square of the gap distance between plates. A 'pull-in' phenomenon, i.e. the deformable plate collapsing onto the ground plate [7,8,13–15], is encountered in such devices. Pull-in instability occurs when the electrostatic force overcomes the elastic restoring force within the plate. The pull-in voltage or collapse voltage [7,14,16] is also known as critical voltage. In some applications, such as micro-switches, pull-in may be desired [13]. In others, tuning the AC frequency and voltage can improve the life expectancy of the device by avoiding pull-in [17,18]. Clamped circular plates, as any other continuous system, have an infinite number of modes of vibration, i.e. mode shapes and their corresponding natural frequencies [16,19–21]. The axisymmetrical modes of vibration depend only on the radial coordinate and not the angular one. In the first axisymmetrical mode of vibration, the entire profile

* Corresponding author.
E-mail addresses: dumitru.caruntu@utrgv.edu, caruntud2@asme-member.org (D.I. Caruntu).

https://doi.org/10.1016/j.ijnonlinmec.2022.104310
Received 4 September 2022; Received in revised form 11 November 2022; Accepted 16 November 2022
Available online 21 November 2022

of the plate deflects in the same direction with the center having the largest deflection while the outer edge has none. A recent review on statics and dynamics of electrically actuated nano and micro structures has been reported in the literature, Khaniki et al. [22]. Also, the same group of researchers reported an investigations on nonlinear size-dependent behavior of electrically actuated MEMS resonators based on the modified couple stress theory [23].

Parametric resonances of micro-structures, such as amplitude–frequency [24–26] and amplitude–voltage [27,28] responses of electrostatically actuated MEMS cantilevers, have been reported in the literature. MEMS behavior has been investigated using different methods. The shooting method, with the applied voltage being an unknown constant function, has been used [12] to facilitate computation to model a clamped circular plate; the results matched experimental data. The Reduced Order Model (ROM) method has been used to transform the partial differential equations of motion into ordinary equations [25,29,30]. The resulting ordinary equations have been solved using the Method of Multiple Scales (MMS) [18], Homotopy Perturbation Method (HPM) [29], or numerical integration [26,31,32].

Investigations on electrostatically actuated MEMS circular plates have been reported in the literature as follows. The static pull-in phenomenon of electrostatically actuated (through a DC voltage) circular micropumps, used in drug delivery systems, has been investigated [32]. Micropump's circular plate has been modeled as a Kirchhoff thin plate. The effects of radius, thickness and initial gap of the micropump on the pull-in voltage have been reported. Von Kármán's nonlinear bending theory of thin plates has been used in this work. Free vibration and static pull-in instability of pre-stressed electrostatically actuated circular microplates to include Casimir force have been reported [33]. The pull-in parameters have been obtained for static deformation of the plate by using the shooting method. Small amplitude free vibrations about the pre-deformed bending configuration have been investigated as well. The effects of the initial gap–thickness ratio, Casimir force, and pre-stress on the pull-in instability and the natural frequency have been reported. An approximate analytical solution of the static deflection of electrostatically actuated thin clamped circular plate has been presented in Ref. [34]. The classical thin-plate theory, valid for adequate large diameter to thickness ratios, situation commonly predominant in MEMS devices, has been used. Galerkin-weighted residual technique has been used under the assumption of small deflections when compared to plate's thickness. The pull-in voltages predicted by the model and ANSYS simulation have been in agreement. Actuation of microplates by fringing electrostatic fields, i.e., field lines between plates and the sidewalls supporting them, has been investigated [35]. This type of actuation is beneficial for operations in open air environment. An analytical model of this actuation principle has been developed and validated numerically using finite element simulations. Due to the absence of small gaps, the device is not disposed to pull-in instability and stiction, and it was not subjected to squeeze-film damping. Humidity and/or dust cannot cause failure. Flow sensors in which a smooth surface is important are excellent applications of this device. Nonlinear resonant behavior of electrostatically actuated micropump circular elastic diaphragms, as they interact with inviscid liquids inside a cylindrical chamber with a central discharge, has been reported in the literature [36]. The partial differential equation of motion includes the nonlinear electrostatic force and the fluid pressure on the diaphragm. MMS has been used to obtain an approximate analytical solution. The system exhibited a softening behavior with DC increase, discharge diameter decrease, and chamber height decrease. Also, electrical and inertial properties of the operating fluid changed the resonant curves significantly.

In this research, the frequency–amplitude response of parametric resonance of electrostatically actuated MEMS clamped circular plates is investigated. The case of axisymmetrical vibrations of plates, which can be used as resonator sensing mechanism, is the focus of this work. The quantum dynamics effects such as Casimir or van der Waals forces are not included. The quantum dynamic effects are significant for gaps lower than 1 μm. Due to the nature of electrostatic actuation, using an AC frequency near natural frequency of the circular plate leads to parametric resonance. First, the partial differential equation of motion is transformed into an ordinary differential equation by using ROM with one term (mode of vibration). Then the ordinary differential equation is integrated using MMS. Second, the partial differential equation of motion is transformed into a system of coupled ordinary differential equations by using ROM with two, three, four, five, six, or seven modes of vibration (or terms). Then the system of the ordinary differential equations is solved numerically using the software package Matlab in order to obtain time responses of the MEMS plate. Also, the system of the ordinary differential equations is solved using AUTO 07P [37], a software package for continuation and bifurcation problems, in order to obtain the frequency–amplitude response.

The motive behind this work is the potential of electrostatically actuated MEMS clamped circular plates to be used as resonator sensors. Parametric resonance constitutes an excellent mechanism for sensing. The sudden jump from a stable zero-amplitude steady-state to large amplitudes up to 0.9 of the gap makes out of the plate resonator an accurate instrument for detecting/sensing biological structures. Bacteria and viruses, which have sizes in the order of micro- and nano-meters are biological structures of interest.

To the best of our knowledge, this is the first time when (1) the amplitude–frequency response of parametric resonance of electrostatically actuated MEMS circular plates is reported, (2) using MMS, numerical integration of ROM with 7 terms using Matlab for time responses, and AUTO 07P. (3) The results of both methods MMS and ROM with 7 terms are in perfect agreement for amplitudes less than 0.5 of the gap, but (5) have significant differences in amplitudes larger than 0.5 of the gap and the gap (pull-in). (6) ROM with 7 terms predicts the instability in high amplitudes (relative to the gap) of the plate, and (7) also predicts a larger interval of frequencies for which the plate can experience pull-in phenomenon if large initial amplitudes. (8) It is shown that the amplitude–frequency interval between the bifurcations of the frequency response increases with the increase of dimensionless voltage and decreases with the increase of the dimensionless damping.

2. Differential equation of motion

The MEMS system under investigation consists of an elastic circular plate, clamped around its outer edge and above a parallel and rigid ground plate (electrode), Fig. 1. The dimensionless equation of axisymmetric vibrations of clamped circular plates, Kirchhoff theory, under electrostatic actuation [16,18,38] is given by

$$\begin{cases} \dfrac{\partial^2 u}{\partial t^2}+\mu\dfrac{\partial u}{\partial t}+\dfrac{\partial^4 u}{\partial r^4}+\dfrac{2}{r}\dfrac{\partial^3 u}{\partial r^3}-\dfrac{1}{r^2}\dfrac{\partial^2 u}{\partial r^2}+\dfrac{1}{r^3}\dfrac{\partial u}{\partial r}=\dfrac{\delta\cos^2\Omega^* t}{(1-u)^2} \\ u(R,t)=\dfrac{\partial u}{\partial r}(R,t)=0 \end{cases} \tag{1}$$

where the dimensionless variables are $u(r,t)$ the dimensionless deflection of current point on the plate, r dimensionless distance from the current point on the plate to the center of the plate, t dimensionless time. The dimensionless parameters are μ the dimensionless damping parameter, δ dimensionless voltage or excitation force parameter, and Ω^* the dimensionless AC frequency. These dimensionless variables and parameters, as well as the flexural rigidity D of the plate, are given by [18]

$$u=\frac{\hat{u}}{d},r=\frac{\hat{r}}{R},t=\hat{t}\sqrt{\frac{D}{\rho h R^4}} \tag{2}$$

$$\mu=2c_1\sqrt{\frac{R^4}{\rho h D}},\quad \delta=\frac{R^4\varepsilon^* V_0^2}{2Dd^3},\quad \Omega^*=\Omega\sqrt{\frac{\rho h R^4}{D}},\quad D=\frac{Eh^3}{12\left(1-\nu^2\right)} \tag{3}$$

where the hat variables in Eq. (2) are the corresponding dimensional variables, R is the outer radius of the elastic uniform circular plate, d the gap between the elastic plate and the ground plate, h the thickness of the elastic plate; and ε^*, E, ν, c_1, V_0 are free space permittivity, Young modulus, Poisson ratio, damping coefficient, and AC voltage amplitude, respectively.

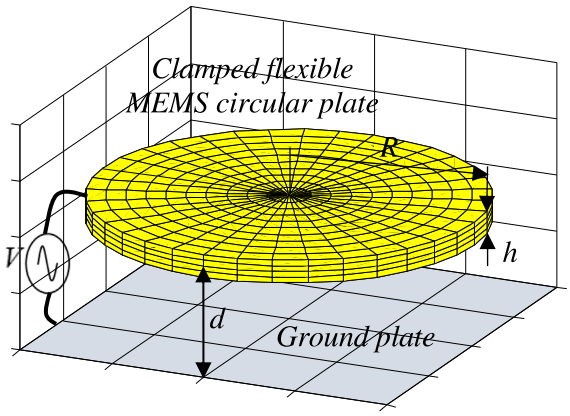

Fig. 1. Uniform flexible MEMS clamped circular plate of radius R and thickness h suspended with a gap d above ground plate.

3. Method of multiple scales

The Method of Multiple Scales (MMS) is an analytical perturbation method that is used in this work to investigate the amplitude–frequency response of the electrostatically actuated MEMS clamped circular plates. MMS is valid only under the assumption that the system is weakly nonlinear and undergoes small deflections. Two time scales [16] are considered in this work, namely fast scale $T_0 = t$ and slow scale $T_1 = \varepsilon t$, where ε is a small bookkeeping parameter. MMS transforms the nonlinear partial differential equation describing the motion of the system into a number of linear ordinary differential equations equal to the number of time scales. In order to use MMS, the electrostatic force in Eq. (1) is expanded in Taylor series. Only terms up to cubic power of the expansion are retained. The dimensionless partial differential equation of motion becomes

$$\frac{\partial^2 u}{\partial t^2} + \varepsilon\mu\frac{\partial u}{\partial t} + P[u] = \varepsilon\delta(1 + 2u + 3u^2 + 4u^3)\cos^2\Omega^* t \tag{4}$$

where the operator P is given by

$$P = \frac{\partial^4}{\partial r^4} + \frac{2}{r}\frac{\partial^3}{\partial r^3} - \frac{1}{r^2}\frac{\partial^2}{\partial r^2} + \frac{1}{r^3}\frac{\partial}{\partial r} \tag{5}$$

The bookkeeping parameter ε [39,40] is used to scale the small nonlinear terms and small damping. The solution u of Eq. (4) that is assumed to be a uniform first order expansion [41] and the time derivative in terms of the time scales are given by

$$u = u_0 + \varepsilon u_1 \quad , \frac{\partial}{\partial t} = D_0 + \varepsilon D_1 \quad D_0 = \frac{\partial}{\partial T_0}, \quad D_1 = \frac{\partial}{\partial T_1} \tag{6}$$

Substituting Eqs. (6) into Eq. (4), expanding the resulting equation, and collecting the ε^0 and ε^1 terms, two problems, namely zero-order and first-order, result as follows

$$\varepsilon^0 : D_0^2 u_0 + P[u_0] = 0 \tag{7}$$

$$\varepsilon^1 : D_0 u_1 + P[u_1] = -2D_0 D_1 u_0 - \mu D_0 u_0 + \delta\left(1 + 2u_0 + 3u_0^2 + 4u_0^3\right)\cos^2\Omega^* T_0 \tag{8}$$

The boundary value problem associated to Eq. (7) gives the solution u_0 [16,18,20,21] as

$$u_0 = \varphi_k(r)\left[A_k(T_1)e^{i\omega_k T_0} + \overline{A}_k(T_1)e^{-i\omega_k T_0}\right] \tag{9}$$

where φ_k is the kth mode shape of vibration and ω_k its corresponding natural frequency [16]. The complex amplitudes $A_k(T_1)$ and its conjugate $\overline{A}_k(T_1)$ are to be determined. The mode shapes φ_k are orthonormal, i.e. $\int_0^1 r\varphi_n(r)\varphi_m(r)dr = \delta_{nm}$, where δ_{nm} is the Kronecker delta, [41]. In this work, the AC frequency Ω^* is near natural frequency ω_k, and it is given by

$$\Omega^* = \omega_k + \varepsilon\sigma \tag{10}$$

where σ is the detuning frequency. One can notice that although the AC frequency is near natural frequency Eq. (10), the excitation frequency of the electrostatic force, which is proportional to the square of the voltage, has a frequency twice the AC frequency. Therefore the MEMS resonator experiences a parametric resonance. In order to solve Eq. (8) for u_1, the solution u_0 given by Eq. (9) is substituted into Eq. (8). One can notice that only one mode of vibration, i.e the kth mode of vibration, is used. Expanding the resulting equation, collecting the secular terms (terms having $e^{i\omega_k T_0}$), and set the sum equal to zero gives the following equation

$$-2\varphi_k A_k' i\omega_k - i\mu\varphi_k\omega_k A_k + \frac{1}{2}\delta\varphi_k\overline{A}_k e^{2i\sigma T_1} + \delta\varphi_k A_k + \delta\varphi_k^3 A_k^3 e^{-2i\sigma T_1} + 3\delta\varphi_k^3 A_k\overline{A}_k^2 e^{2i\sigma T_1} + 6\delta\varphi_k^3 A_k^2\overline{A}_k = 0 \tag{11}$$

where $A_k' = dA_k/dT_1$, i.e. the rate of change of A_k with respect to the slow scale T_1. Substituting the polar form of the complex coefficients $A_k = a_k e^{i\theta_k}/2$ and $\overline{A}_k = a_k e^{-i\theta_k}/2$, where a_k and θ_k are the real amplitude and phase, respectively, into Eq. (11), the Galerkin method is then used by multiplying the resulting equation by r and $\varphi_k(r)$ and integrating from 0 to 1. The imaginary and real parts of the resulting equation are separated into two equations used afterwards to obtain the amplitude–frequency (a_k, σ) slow scale differential equations. The steady-state solutions, which require no change with respect to the slow scale T_1, are found using $a_k' = \gamma_k' = 0$, where $\gamma_k = \sigma T_1 - \theta_k$, [16]. The amplitude–frequency response consists of steady-state amplitudes $a_k = 0$ for all considered σ, and non-zero steady-state amplitudes given by

$$a_k = \sqrt{\frac{2\mu\omega_k g_{2k}}{\delta g_{4k}\sin 2\gamma_k} - \frac{g_{2k}}{g_{4k}}} \tag{12}$$

$$\sigma = -\frac{1}{4\omega_k}\left[\left(2 + \cos 2\gamma_k\right)\delta + \frac{g_{4k}}{g_{2k}}\left(2\delta\cos 2\gamma_k + 3\delta\right)a_k^2\right] \tag{13}$$

where

$$g_{ik} = \int_0^1 r\varphi_k^i(r)dr \tag{14}$$

In the numerical simulations to follow, $k = 1$, i.e. the AC frequency is near the first natural frequency.

4. Reduced order models

Reduced Order Models (ROMs) to include several modes of vibration consist of systems of ordinary differential equations. ROM's system of ordinary differential equations is (1) numerically integrated [42] to predict time responses of the MEMS resonator, and (2) solved using the continuation and bifurcation method to predict the amplitude–frequency response. ROMs are not limited to the assumption of weak nonlinearities. Therefore, ROMs can be used to accurately predict the response for both low and high amplitude vibrations. ROMs using a larger number of modes of vibration give better predictions in high amplitudes of the pull-in instabilities and steady-states amplitudes. The deflection at any point of the circular plate, Eq. (1), can be described by [18]

$$u(r,t) = \sum_{i=1}^{N} u_i(t)\varphi_i(r) \tag{15}$$

where the number of modes of vibration (terms) N of the ROM is finite, and the dimensionless displacement $u(r,t)$ is a function of the mode shapes $\varphi_i(r)$ [18]. Time-dependent functions $u_i(t)$ are to be determined through numerical integration of the system of differential equations describing the motion of the plate. The partial differential equation of motion Eq. (1) is multiplied by $(1-u)^2$ in order to eliminate all denominators and reduce the computational cost [16,43]. Replacing Eq. (15) into the resulting equation, and then multiplying the resulting

Table 1
First seven natural frequencies for clamped circular plate.

	$N=1$	$N=2$	$N=3$	$N=4$	$N=5$	$N=6$	$N=7$
ω_k	10.216	39.771	89.104	158.183	247.005	355.568	483.872

Table 2
Dimensional system parameters.

Radius of plate	R	250.0	μm
Initial gap distance	d	1.014	μm
Plate thickness	h	3.01	μm
Permittivity of free space	ε^*	8.854e−12	$C^2/N/m^2$
Young's modulus	E	150.6	GPa
Poisson's ratio	ν	0.0436	
Density of material	ρ	2330.0	kg/m^3
Damping	c_1	1.962	Ns/m^3
Voltage	V_0	2.035	V

equation by r and $\varphi_k(r)$ and integrating from 0 to 1 (Galerkin method), the following system of N differential equations, $n = 1, 2, \ldots, N$, result

$$\sum_{i=1}^{N} A_{ni}\frac{\partial^2 u_i}{\partial t^2} = -\mu\sum_{i=1}^{N} A_{ni}\frac{\partial u_i}{\partial t} - \sum_{i=1}^{N} A_{ni}\omega_i^2 u_i + \delta h_n \cos^2\Omega^* t \tag{16}$$

where $A_{ni} = \sum_{jk}^{N} h_{nijk}u_j u_k - 2\sum_{j}^{N} h_{nij}u_j + h_{ni}$
and

$$h_n = \int_0^1 r\varphi_n dz, \quad h_{ni} = \int_0^1 r\varphi_n\varphi_i dz,$$
$$h_{nij} = \int_0^1 r\varphi_n\varphi_i\varphi_j dz, \quad h_{nijk} = \int_0^1 r\varphi_n\varphi_i\varphi_j\varphi_k dz \tag{17}$$

This work investigates the amplitude–frequency response of the circular plate for AC frequency near natural frequency of the plate. Therefore, the excitation frequency Ω^* used in ROMs is given by Eq. (10) for $\varepsilon = 1$. The resulting system of N second order differential Eqs. (16) is transformed into a system of $2N$ first order differential equations. This system is then solved using AUTO 07 for $N = 2, 3, 4, 5, 6, 7$ number of modes (terms) in order to investigate the convergence of ROMs amplitude–frequency responses. AUTO 07 is a software package for continuation and bifurcation problems [36]. Moreover, the behavior of the system is also tested finding time responses by direct integration of ROMs using Matlab. Specifically, the system of $2N$ first-order differential equations is integrated in order to predict the steady-state amplitudes of the center of the MEMS circular plate resonator. The amplitude–frequency response is necessary for understanding the relationship between the steady-state amplitudes of vibration and the applied excitation frequencies. The effects of voltage and damping parameters on the amplitude–frequency response are reported. Numerical results from MMS, ROM using AUTO 07, and ROM using Matlab, are compared in the next section.

5. Numerical simulations

Numerical simulations are conducted for predicting the amplitude–frequency response of electrostatically actuated MEMS circular plate resonators. They are conducted for typical MEMS circular plate resonators in rarefied gas. First seven dimensionless natural frequencies of axisymmetric vibrations of clamped uniform circular plates are given in Table 1. The dimensionless natural frequencies resulted from solving the frequency equation of clamped circular plates [16]. The dimensions and constants of a typical electrostatically actuated MEMS circular plate resonator, with negligible Casimir forces [44] as the gap distance is larger than 1 μm, are given in Table 2. Poisson ratio of silicon is also included [45]. Using Table 2, the dimensionless parameters δ and μ are calculated and given in Table 3.

The amplitude–frequency response of electrostatically actuated clamped circular plates, with AC frequency near first natural frequency, $k = 1$ in Eqs. (9), (10), (12), (13), of the plate, is analytically and

Table 3
Dimensionless system parameters.

Electrostatic constant	δ	0.200
Damping constant	μ	0.005

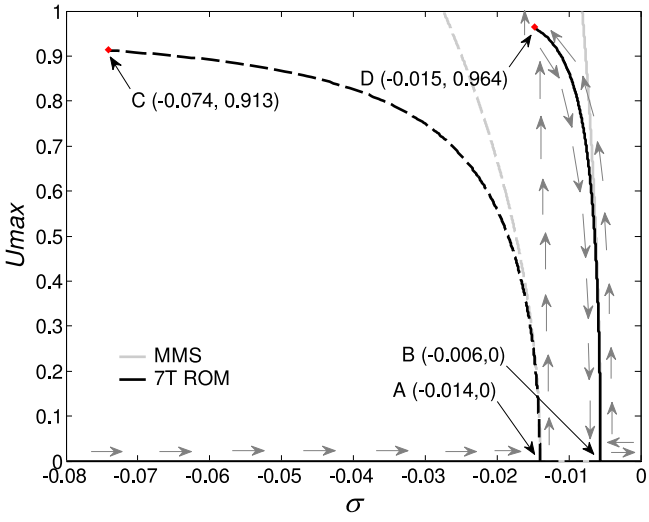

Fig. 2. Frequency response of clamped circular plate excited near natural frequency using MMS and 7T ROM AUTO. $\delta = 0.2$, $\mu = 0.005$.

numerically predicted, Fig. 2. The frequency of actuation is twice the AC frequency since the force of excitation is proportional to V^2, therefore the resonance experienced by the MEMS plate is parametric resonance. Phase–frequency response [46] is not included in this work. The coefficients given by Eq. (12), (13) and used in these simulations are $g_{11} = 0.5155$, $g_{21} = 1.0005, g_{31} = 2.3381$, $g_{41} = 5.9763$. (1) MMS using Eq. (12), (13) for amplitude–frequency response, (2) ROM of seven modes of vibration (7T), $N = 7$ in Eqs. (16), using AUTO 07 for amplitude–frequency response, and (3) ROM of seven modes of vibration (7T) using Matlab to numerically integrate and predict time responses, are used to predict amplitude–frequency response of the parametric resonance.

Fig. 2 shows the amplitude–frequency response of the parametric resonance of electrostatically actuated MEMS circular plates using MMS and seven modes (7T) ROM AUTO 07. This response consists of steady-state solutions of the MEMS plate resonator vibrating motion, i.e. the dimensionless steady-state amplitude of the center of the MEMS plate *Umax* versus the dimensionless detuning frequency of actuation σ. The steady-state solutions are either stable or unstable. The stable solutions are represented by solid lines, and unstable solutions by dash lines. Two bifurcations, subcritical and supercritical, specific to parametric resonance occur. Points *A* and *B* are bifurcation points, i.e. points where the stability changes. Point *A* is the bifurcation point of the subcritical bifurcation which consists of zero steady-state solutions branch that is stable for frequencies less than the frequency of point *A* and unstable for larger frequencies, and unstable branch *AC*. One can notice that *C* is the end point in high amplitudes of the unstable branch *AC*. Point *B* is the bifurcation point of the supercritical bifurcation which consists of zero steady-state solutions branch that is unstable for frequencies less than the frequency of *B* and stable for larger frequencies, and stable branch *BD*. It can be seen that *D* is the end point in high amplitudes of branch *BD*. Zero steady-state amplitudes occur at all frequencies under investigation, Fig. 2, and they are unstable between the bifurcation points *A* and *B*, and stable elsewhere within the investigated range of frequencies. The bending of the stable and unstable non-zero steady-state amplitude branches *BD* and *AC* to the left (lower frequencies) shows that the system experiences a softening effect. So, for stable steady-state amplitude branch, one can see that the physics of this is

the phenomenon in which the frequency of vibration decreases with the increase in amplitude.

A comparison between the three methods used (1) MMS of ROM using one mode of vibration, (2) ROM using seven modes of vibration solved using the continuation and bifurcation method, and (3) ROM using seven modes of vibration numerically integrated, shows that they are in good agreement predicting the subcritical and supercritical bifurcations, their bifurcation points *A* and *B*, and the softening effect of the response. Specifically, all three methods are in perfect agreement for dimensionless amplitudes less than 0.5, i.e. dimensional amplitudes less than half the gap. However, for dimensionless amplitudes between 0.5 and 1.0, i.e. dimensional amplitudes larger than half the gap but less than the gap, MMS underestimates the softening effect failing to predict the behavior of the system. MMS is limited to small amplitudes and small nonlinearities. In this range of amplitudes, ROM method using seven modes of vibration predicts the behavior of the MEMS plate. The endpoints of the unstable and stable branches, point C and point D, are only predicted by ROM using seven modes of vibration. MMS does not predict the pull-in phenomenon that occurs at high amplitudes, i.e. point *D*. However, using MMS one can rapidly evaluate the type of amplitude–frequency response.

Regarding the physics behind Fig. 2, there are two cases to be discussed. First case to be discussed is concerned with the steady-state amplitudes of the MEMS plate at constant voltage as the frequency is swept up or swept down. The discussion is further conducted based on the seven modes of vibration ROM AUTO 07 results. As the frequency is swept up (moving from lower to higher frequency values) the steady-state amplitude remains zero until it reaches the subcritical bifurcation point *A* where it loses stability and jumps to the high amplitude stable solution branch *BD*. As the frequency continues to increase, the steady-state amplitude decreases along branch *BD* until it reaches the supercritical bifurcation point *B* of zero amplitude, and then continues to have zero amplitude. Arrows from low frequency in the succession right-up-down-right show this behavior. As the frequency is swept down, the steady-state amplitudes are zero until the bifurcation point *B* is reached. Then the amplitude increases along the stable branch *BD* until it reaches point *D* where the MEMS plate resonator loses stability and jumps to an amplitude of one, experiencing a pull-in phenomenon. Arrows from high frequency in the succession left-up-jump to *Umax = 1* show this behavior. One should notice that sweeping down the frequency forces the system always to pull-in.

Second case is when the voltage and the frequency are constant and the initial amplitude of the MEMS plate resonator is given. This discussion shows the importance of the initial amplitude on the response of the MEMS plate resonator. Several time response simulations have been conducted, Fig. 3, in order to test the frequency response given in Fig. 2. One can notice the agreement between Fig. 3 and Fig. 2.

If the frequency is less than σ_C the frequency of point *C*, then regardless of the initial amplitude, which has to be less than one, the system settles to a zero steady-state amplitude. Fig. 3a shows additional testing by simulating the time response of such point. Matlab is used to solve the 7T ROM in the case of frequency $\sigma = -0.075$ and initial amplitude of $U_0 = 0.95$, and parameters $\delta = 0.2$, $\mu = 0.005$. The frequency and the initial amplitude locate the initial position at the left-hand side and above of point *C*. As seen in Fig. 3a, the amplitude settles to zero *Umax = 0*. It can be concluded that the unstable branch *AC* does not exist at $\sigma = -0.075$, therefore $\sigma_C > -0.075$.

If the frequency is between σ_C and σ_D, and the initial amplitude is above the unstable branch *AC*, the MEMS plate experiences pull-in. Fig. 3b shows additional testing by simulating the time response of such point, i.e. frequency $\sigma = -0.07$ and initial amplitude of $U_0 = 0.95$, and parameters $\delta = 0.2$, $\mu = 0.005$. The frequency and the initial amplitude locate the initial position at the right-hand side and above of point *C*. One can notice that the amplitude increases until it reaches *Umax = 1*, i.e. pull-in. One can conclude that the unstable branch exists at $\sigma = -0.07$, therefore $\sigma_C < -0.07$.

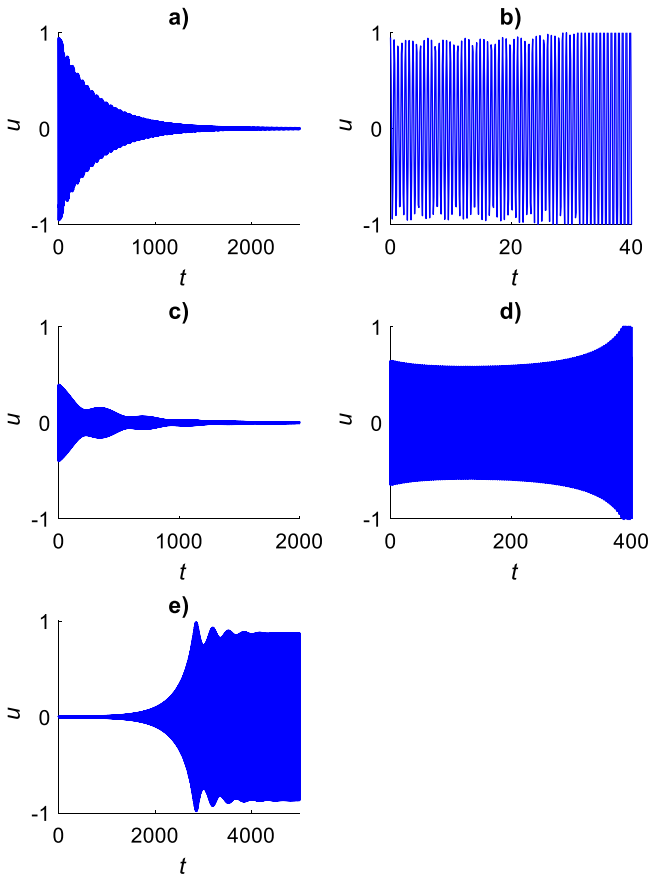

Fig. 3. Time response for MEMS clamped circular plate for 7T ROM. AC near natural frequency. (a) $\delta = 0.2$, $\mu = 0.005$, $\sigma = -0.075$. Initial amplitude $U_0 = 0.95$; (b) $\delta = 0.2$, $\mu = 0.005$, $\sigma = -0.07$. Initial amplitude $U_0 = 0.95$; (c) $\delta = 0.2$, $\mu = 0.005$, $\sigma = -0.02$. Initial amplitude $U_0 = 0.4$; (d) $\delta = 0.2$, $\mu = 0.005$, $\sigma = -0.02$. Initial amplitude $U_0 = 0.65$; (e) $\delta = 0.2$, $\mu = 0.005$, $\sigma = -0.012$. Initial amplitude $U_0 = 0$.

To summarize, Figs. 3a and 3b are in agreement with Fig. 2. They also show that that point *C* exists and its frequency σ_C is between -0.075 and -0.07. This is in agreement with $\sigma_C = -0.074$ predicted by AUTO ROM 7T in Fig. 2.

If the frequency is between σ_C and σ_A, and the initial amplitude U_0 is under the unstable branch *AC*, the MEMS plate settles to a zero steady-state amplitude *Umax = 0*. For an initial amplitude U_0 above the unstable branch in this case, the MEMS plate goes into pull-in *Umax = 1*. Figs. 3c and 3d show further testing by simulating the time responses of such points. The time responses for the cases of two points in Fig. 2 having the same frequency $\sigma = -0.02$, and initial amplitudes $U_0 = 0.4$ below and $U_0 = 0.65$ above unstable branch *AC,* are shown in Fig. 3c and Fig. 3d respectively. Both figures use the same parameters $\delta = 0.2$, $\mu = 0.005$. Figs. 3c and 3d show that for an initial amplitude U_0 below the unstable branch the system settles to zero amplitude *Umax = 0*, while for an initial amplitude U_0 above the unstable branch the system goes into pull-in *Umax = 1*. This is in agreement with the existence of the unstable branch *AC* in Fig. 2. If the frequency is between σ_A and σ_B, regardless the initial amplitude, the MEMS plate settles to an amplitude on the stable branch *BD*. Fig. 3e shows further testing by simulating the time response of such a point, i.e. frequency $\sigma = -0.012$ and initial amplitude of $U_0 = 0$, and parameters $\delta = 0.2$, $\mu = 0.005$. One can see that the amplitude increases until it reaches steady-state amplitude *Umax = 0.87*, which is in perfect agreement with Fig. 2, this steady-state point being on the stable branch *BD*.

Fig. 4 illustrates the convergence of the ROM method using AUTO 07. The convergence of the ROM by the number $N = 2, 3, 4, 5, 6, 7$ of

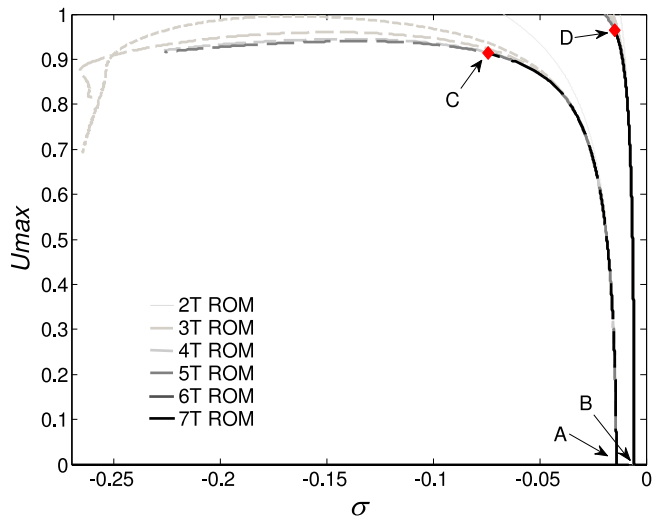

Fig. 4. Frequency response for a clamped circular plate showing the convergence of ROM from 2 to 7 terms. $\delta = 0.2$, $\mu = 0.005$.

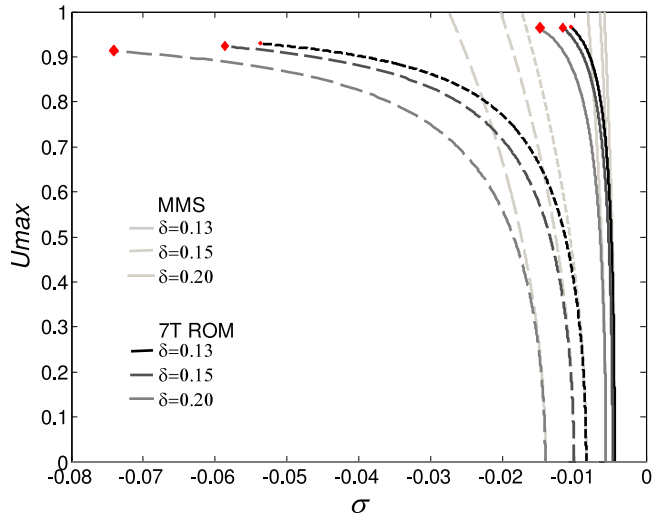

Fig. 5. Frequency response for a clamped circular plate using MMS and ROM showing the influence of the excitation parameter δ at natural frequency and damping parameter held constant at $\mu = 0.005$.

modes of vibration considered in the model is shown. One can see that for amplitudes below *Umax = 0.8* of the gap, regardless the number of modes $N = 2, 3, 4, 5, 6, 7$ used, ROMs predict the same behavior (same branches). However, for amplitudes larger than *Umax = 0.8* of the gap, only ROM using seven modes of vibration (7T-ROM), $N = 7$, predicts the unstable point *D* of the stable branch *BD*, and the end point *C* of the unstable branch *AC*. These two points *C* and *D* are important since they show the range of frequencies and initial amplitudes for pull-in, stable non-zero amplitudes, and stable zero amplitudes. One can conclude that to be able to predict the response in both small and large amplitudes 7T-ROM has to be used. A similar converge investigation has been conducted in Ref. [18] for primary resonance. One should mention that larger number of modes of vibration in the ROM comes with a significant computational cost.

Next, the effects of voltage δ and damping μ parameters on the amplitude–frequency response are investigated, Figs. 5 and 6–8, respectively.

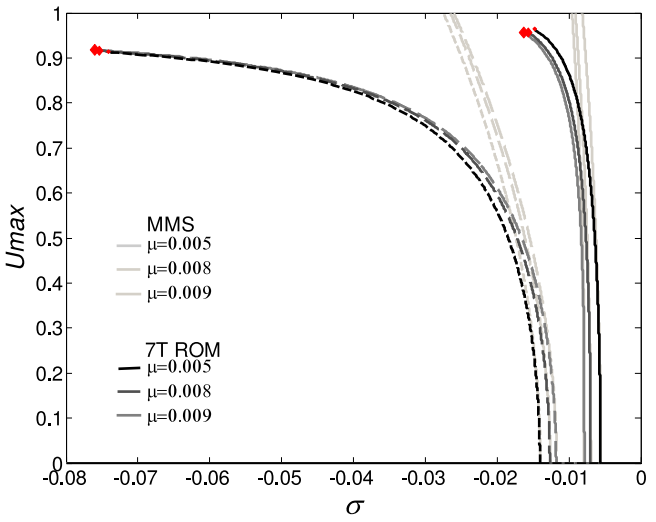

Fig. 6. Frequency response for a clamped circular plate using MMS and ROM showing the influence of the damping parameter μ at natural frequency and excitation parameter held constant at $\delta = 0.2$.

Fig. 5 shows three cases $\delta = 0.13$, $\delta = 0.15$, and $\delta = 0.2$, and two methods of investigation, namely MMS and 7T-ROM AUTO 07. As the voltage parameter δ increases, the subcritical and supercritical bifurcations, points *A* and *B*, respectively, shift to lower frequencies. Between the two bifurcation points, point *A* shifts significantly, increasing the range of frequency for which, regardless the initial amplitude U_0, the amplitude of the MEMS plate settles to a steady-state solution *Umax* on branch *BD,* or to *Umax = 1* experiencing pull-in. The endpoint *C* of the unstable branch is also shifted to lower frequencies, giving a larger range of frequencies for which pull-in can be achieved if the initial amplitude is above the unstable branch. The pull-in instability point *B* remains at the same amplitude while shifting to lower frequencies. MMS fails to predict the behavior of the MEMS plate above *Umax = 0.5* of the gap.

Fig. 6 shows the effect of damping on the amplitude–frequency response using MMS and 7T ROM AUTO 07. Three cases $\mu = 0.005$, $\mu = 0.008$, and $\mu = 0.009$ are showed. At lower amplitudes there is a significant difference between the 3 cases. The subcritical and supercritical bifurcation points *A* and *B* get closer as the damping increases, reducing the interval of frequencies for which the MEMS plate can reach large amplitudes on branch *BD* or pull-in from an initial amplitude $U_0 = 0$. For a given frequency $\sigma = -0.01$, the amplitude decreases with the increase of damping. For instance, $\mu = 0.005$ gives *Umax = 0.86*, $\mu = 0.008$ gives *Umax = 0.8*, and $\mu = 0.009$ gives *Umax = 0.76*.

Also, as the damping increases, both end points *C* and *D* are shifted to lower frequencies, Figs. 7 and 8. Although the change of the values of dimensionless detuning frequencies σ of points *C* and *D* seem to be small, the dimensional frequency changes are in the order of thousands of Hz, Eqs. (3) and (12).

6. Discussion and conclusions

This work investigates the amplitude–frequency response of parametric resonance of electrostatically actuated clamped MEMS uniform circular plate resonators. The frequency of the actuating AC voltage is near natural frequency. DC voltage is not considered in this work. However, one should mention that the existence of additional DC voltage in the system changes the type of bifurcation [47]. Three methods of investigation, analytical, continuation and bifurcation, and numerical integration, namely MMS, continuation and bifurcation, and

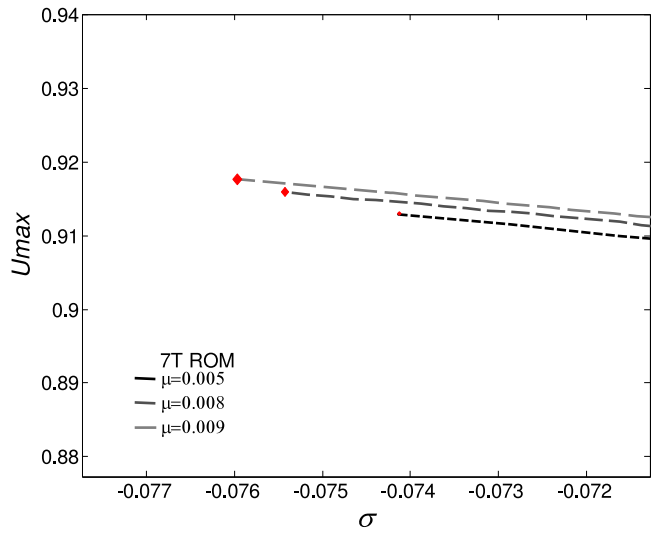

Fig. 7. Zoom in of unstable branches from Fig. 6.

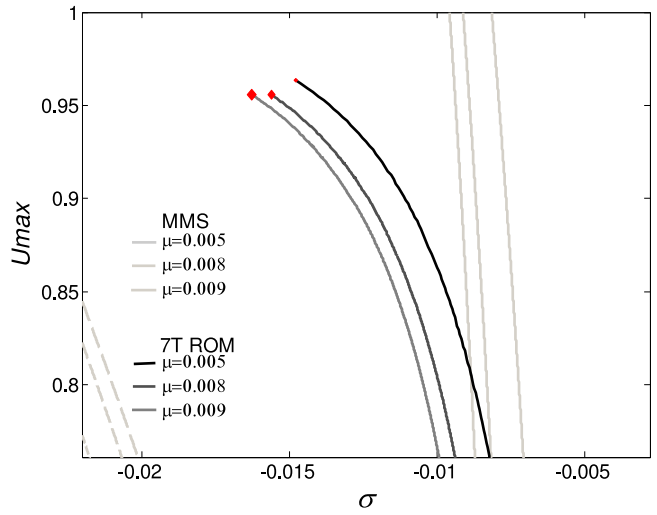

Fig. 8. Zoom in of stable branches from Fig. 6.

numerical integration, respectively, are used. The system is first modeled using one term (mode of vibration) reduced order model which is then analytically solved using a perturbation method, i.e. MMS. Secondly, the system is modeled using two, three, four, five, six, and seven terms (modes of vibration) ROMs and solved using the continuation and bifurcation software package AUTO 07 in order to obtain the amplitude–frequency responses. The parametric resonance is additionally tested by numerically integrating seven terms (modes of vibration) ROM using Matlab to obtain time responses of the MEMS plate resonator. MMS and ROM are in perfect agreement for steady-state amplitudes less than 0.5 of the gap. For larger amplitudes MMS fails since MMS is valid for systems with weak nonlinearities and small amplitudes. One can improve to some extent the predictions of MMS in higher amplitudes by increasing the degree of the Taylor polynomial approximating the electrostatic force [48] and/or by using a second order expansion in Eq. (6). However, by approximating the electrostatic force with Taylor polynomials, regardless the expansion order, the singular points are lost. Therefore, MMS cannot predict points *C* and *D*, Fig. 2. Although MMS is limited, it proves to be an effective and reliable method for investigating the amplitude–frequency response of a system at small amplitudes. An investigation regarding the convergence of ROM with respect to the number of terms included shows that seven terms are necessary to accurately model the response of the MEMS plate at high amplitudes and pull-in instability. The simulated time responses of the system show a perfect agreement with the amplitude–frequency response using seven terms ROM AUTO 07. One should mention that predicting accurately the unstable branch *AC* is important since disturbances such as mechanical shock [31,49,50] or spike of undesired direct current (DC) voltage on the structure can occur leading to amplitudes above *AC*, so MEMS plate is accidentally led to pull-in.

This work is valid for (1) axisymmetrical vibrations, (2) small amplitudes when compared to the thickness of the plate (no geometrical nonlinearities), (3) gaps larger than 1 μm (not significant quantum dynamics effects such as Casimir or Van der Waals forces), and (4) linear damping, of uniform MEMS plate resonators.

The effects of voltage and damping on the amplitude–frequency response are reported. Increasing the voltage parameter δ results in shifting of subcritical and supercritical bifurcations to lower frequencies, subcritical significantly more than supercritical. Increasing the damping coefficient μ results in narrowing the frequency range between the subcritical and supercritical bifurcation points.

The numerical simulations of this work are valid only for squeeze damping in rarefied gas [10]. The energy transfer model of quality factor Q [10] along with the MEMS resonator characteristics in Table 2 gave the value of damping parameter in Table 3. For the first mode of vibration, as in this paper, this corresponds to a pressure of 1000 Pa.

Numerical simulations in this work are consistent with the assumption of linear damping. First, using data from Table 2, the mean free path $\lambda = K_B \cdot T / \left(\sqrt{2}\pi P d_m^2\right)$ and Knudson number $Kn = \lambda/d$ can be determined [10]. Second, the effective viscosity [10] $\mu_{eff} = \mu / \left(1 + 9.658 \cdot Kn^{1.159}\right)$ due to rarefied gas is determined. Finally, the squeeze number [10] $\sigma = 12\mu_{eff} \cdot \omega \cdot R^2 / \left(P \cdot d^2\right)$, for the frequency of vibration of the MEMS plate, results as $\sigma = 1.115 \cdot 10^{-4}$. For this squeeze number, the damping is linear according to the data reported in the literature. Bao and Yang [10] reported the relationship between viscous damping force and the squeeze number. According to Ref. [10], for $\sigma \in (0, 1)$ the viscous damping is linear, and the elastic component of the squeeze film is negligible.

If one would investigate highly nonlinear problems, superharmonic and subharmonic resonances, then a ROM using seven modes of vibration would have accurate predictions in both lower and higher amplitudes. However, MMS using one mode of vibration would fail to accurately predict the behavior of the plate in high amplitudes. One could also use three time scales for MMS and different ordering of the nonlinear terms and damping [42]. However, this will not produce accurate results for large amplitudes, since MMS is limited to weak nonlinear systems and small amplitudes. ROM with sufficient number of modes of vibration accurately predict the behavior of the structure [18].

Limitations of this work include (1) lack of experimental validation, (2) the use of "Kirchhoff plate theory (classical plate theory) valid for thin plates, i.e. thickness to diameter radius ratio less than 0.05" [48], so the results of this work do not apply to thick plates or plates with geometrical nonlinearities, and (3) the investigation of only axisymmetric MEMS plate vibrations.

Future work would include non-axisymmetrical vibrations, quantum dynamics effects (Casimir or Van der Waals), large amplitudes (geometrical nonlinearities), non-uniform plates, modal interactions and secondary resonances [51,52]. Dynamic modal characteristics of nonuniform structures, or methods to find such characteristics are reported in the literature [53–55]. The quantum dynamics effects are significant for gaps lower than 1 μm [48,56].

Declaration of competing interest

The authors declare that they have no known competing financial interests or personal relationships that could have appeared to influence the work reported in this paper.

Data availability

Data will be made available on request.

Acknowledgements

This material is based on research sponsored by Air Force Research Laboratory under agreement number FA8650-07-2-5061. The U.S. Government is authorized to reproduce and distribute reprints for Governmental purposes notwithstanding any copyright notation thereon. The views and conclusions contained herein are those of the authors and should not be interpreted as necessarily representing the official policies or endorsements, either expressed or implied, of Air Force Research Laboratory or the U.S. Government.

References

[1] A.R.H. Goodwin, A.D. Fitt, K.A. Ronaldson, W.A. Wakeham, A vibrating plate fabricated by the methods of microelectromechanical systems (MEMS) for the simultaneous measurement of density and viscosity: Results for argon at temperatures between 323 and 423K at pressures up to 68 MPa, Int. J. Thermophys. 27 (6) (2006) 1650–1676.

[2] A.R.H. Goodwin, E.P. Donzier, O. Vancauwenberghe, M. Manrique de Lara, F. Marty, B. Mercier, A.D. Fitt, K.A. Ronaldson, W.A. Wakeham, A vibrating edge supported plate, fabricated by the methods of micro-electro-mechanical-system for the simultaneous measurement of density and viscosity: Results for methylbenzene and octane at temperatures between (323 and 423) K and pressures in the range (0.1 to 68) MPa, J. Chem. Eng. Data 51 (1) (2006) 190–208.

[3] S. Cerimovic, R. Beigelbeck, H. Antlinger, J. Schalko, B. Jakoby, F. Keplinger, Sensing viscosity and density of glycerol–water mixtures utilizing a suspended plate MEMS resonator, Microsyst. Technol. 18 (7–8) (2012) 1045–1056.

[4] P. Helistö, H. Sipola, H. Seppä, A.J. Manninen, MEMS-based voltage detector, Sensors Actuators A 234 (1) (2015) 99–103.

[5] A.A. Trusov, A.M. Shkel, Parallel plate capacitive detection of large amplitude motion in MEMS, in: Proceedings of the 14th International Conference on Solid-State Sensors, Actuators and Microsystems, Lyon, France, June 10-14, 2007, pp. 1693–1696.

[6] R.E. Speight, M.A. Cooper, A survey of the 2010 quartz crystal microbalance literature, J. Mol. Recognit. 25 (1) (2012) 451–473.

[7] B. Ahmad, R. Pratap, Elasto-electrostatic analysis of circular microplates used in capacitive micromachined ultrasonic transducers, IEEE Sens. J. 10 (11) (2010) 1767–1773.

[8] K. Rashvand, G. Rezazadeh, H. Mobki, M. Ghayesh, On the size-dependent behavior of a capacitive circular micro-plate considering the variable length-scale parameter, Int. J. Mech. Sci. 77 (1) (2013) 333–342.

[9] A. Soma, G. De Pasquale, Numerical and experimental comparison of MEMS suspended plates dynamic behaviour under squeeze film damping effect, Analog Integr. Circuits Signal Process. 57 (3) (2008) 213–224, http://dx.doi.org/10.1007/s10470-008-9165-x.

[10] M. Bao, H. Yang, Squeeze film air damping in MEMS, Sensors Actuators A 136 (1) (2007) 3–27.

[11] L. Mol, L.A. Rocha, E. Cretu, R.F. Wolffenbuttel, Squeezed film damping measurements on a parallel-plate MEMS in the free molecule regime, J. Micromech. Microeng. 19 (7) (2009) 074021, (6 pages).

[12] Y. Wang, W. Lin, X. Li, Z. Feng, Bending and vibration of an electrostatically actuated circular microplate in presence of Casimir force, Appl. Math. Model. 35 (5) (2011) 2348–2357.

[13] W. Zhang, H. Yan, Z. Peng, G. Meng, Electrostatic pull-in instability in MEMS/NEMS: A review, Sensors Actuators A 214 (1) (2014) 187–218.

[14] W. Zhang, G. Meng, D. Chen, Stability, nonlinearity and reliability of electrostatically actuated MEMS devices, Sensors 7 (1) (2007) 760–796.

[15] G.N. Nielson, G. Barbastathis, Dynamic pull-in of parallel-plate and torsional electrostatic MEMS actuators, J. Microelectromech. Syst. 15 (4) (2006) 811–821.

[16] D.I. Caruntu, R. Oyervides, Primary resonance voltage response of electrostatically actuated MEMS clamped circular plate resonators, J. Comput. Nonlinear Dyn. 11 (4) (2016) 041021, (7pages).

[17] F. Lakrad, M. Belhaq, Suppression of pull-in in a microstructure actuated by mechanical shocks and electrostatic forces, Int. J. Non-Linear Mech. 46 (2) (2011) 407–414.

[18] D.I. Caruntu, R. Oyervides, Frequency response reduced order model of primary resonance of electrostatically actuated MEMS circular plate resonators, Commun. Nonlinear Sci. Numer. Simul. 43 (1) (2017) 261–270.

[19] A. Gualdino, V. Chu, J. Conde, Multi-modal analysis of out-of-plane vibration modes of thin-film circular resonators for mass sensing applications, Procedia Eng. 47 (1) (2012) 1121–1124.

[20] S.S. Rao (Ed.), Vibration of Continuous Systems, John Wiley & Sons, Hoboken, New Jersey, USA, 2007.

[21] A.W. Leissa, Vibration of Plates, Acoustic Society of America (Originally published 1969 by Washington: Office of Technology Utilization, NASA SP-160), 1993.

[22] H.B. Khaniki, M.H. Ghayesh, M. Amabili, A review on the statics and dynamics of electrically actuated nano and micro structures, Int. J. Non-Linear Mech. 129 (2021) 103658, (33 pages).

[23] M.H. Ghayesh, H. Farokhi, M. Amabili, Nonlinear behaviour of electrically actuated MEMS resonators, Internat. J. Engrg. Sci. 71 (2013) 137–155.

[24] D.I. Caruntu, M. Knecht, Microelectromechanical systems cantilever resonators under soft alternating current voltage of frequency near natural frequency, J. Dyn. Syst. Meas. Control 137 (4) (2015) 041016, http://dx.doi.org/10.1115/1.4028887, (8pp).

[25] D.I. Caruntu, I. Martinez, Reduced order model of parametric resonance of electrostatically actuated MEMS cantilever resonators, Int. J. Non-Linear Mech. 66 (1) (2014) 28–32.

[26] D.I. Caruntu, E. Juarez, Voltage effect on amplitude–frequency response of parametric resonance of electrostatically actuated double-walled carbon nanotube resonators, Nonlinear Dynam. 98 (4) (2019) 3095–3112, http://dx.doi.org/10.1007/s11071-019-05057-8.

[27] D.I. Caruntu, I. Martinez, M.W. Knecht, Parametric resonance voltage response of electrostatically actuated micro-electro-mechanical system cantilever resonators, J. Sound Vib. 362 (1) (2016) 203–213.

[28] D.I. Caruntu, E. Juarez, Coaxial vibrations of electrostatically actuated DWCNT resonators: Amplitude–voltage response of parametric resonance, Int. J. Non-Linear Mech. 142 (2022) 103982, http://dx.doi.org/10.1016/j.ijnonlinmec.2022.103982, (8 pages).

[29] M. Mojahedi, M. Moghimi Zand, M.T. Ahmadian, Static pull-in analysis of electrostatically actuated microbeams using homotopy perturbation method, Appl. Math. Model. 34 (4) (2010) 1032–1041.

[30] N. Sharafkhani, G. Rezazadeh, R. Shabani, Study of mechanical behavior of circular FGM micro-plates under nonlinear electrostatic and mechanical shock loadings, Acta Mech. 223 (3) (2012) 579–591.

[31] G. Vogl, A.H. Nayfeh, A reduced order model for electrically actuated clamped circular plates, J. Micromech. Microeng. 15 (1) (2005) 684–690.

[32] F.C. Rahim, A numerical approach to investigate of pull-in phenomenon of circular micro plate subjected to nonlinear electrostatic pressure, Sens. Transducers 117 (6) (2010) 41–49.

[33] Y.-G. Wang, W.-H. Lin, X.-M. Li, Z.-J. Feng, Bending and vibration of an electrostatically actuated circular microplate in presence of casimir force, Appl. Math. Model. 35 (5) (2011) 2348–2357.

[34] B. Ahmad, R. Pratap, Elasto-electrostatic analysis of circular microplates used in capacitive micromachined ultrasonic transducers, IEEE Sensors 10 (11) (2010) 1767–1773.

[35] A. Rabinovich, A. Yaakobovitz, S. Krylov, Fringing electrostatic field actuation of microplates for open air environment sensing, J. Vib. Acoust. 136 (4) (2014) 041013, (10 pages).

[36] M. Sheikhlou, R. Shabani, G. Rezazadeh, Nonlinear analysis of electrostatically actuated diaphragm-type micropumps, Nonlinear Dynam. 83 (1–2) (2016) 951–961.

[37] E.J. Doedel, B.E. Oldeman, AUTO-07P: Continuation and Bifurcation Software for Ordinary Differential Equations, Concordia University, Montreal, Canada, 2009.

[38] J.A. Pelesko, D.H. Bernstein, Modeling MEMS and NEMS, Chapman & CRC Hall/CRC, Boca Raton, 2003.

[39] M.I. Younis, A.H. Nayfeh, A study of the nonlinear response of a resonant microbeam to electric actuation, Nonlinear Dynam. 31 (1) (2003) 91–117.

[40] A.H. Nayfeh, Introduction to Perturbation Techniques, Wiley, New York, 1981.

[41] D.I. Caruntu, L. Luo, Frequency response of primary resonance of electrostatically actuated CNT cantilevers, Nonlinear Dynam. 78 (3) (2014) 1827–1837.

[42] A.H. Nayfeh, D.T. Mook, Nonlinear Oscillations, Wiley, New York, 1979.

[43] M.I. Younis, H.M. Ouakad, F.M. Alsaleem, R. Miles, W. Cui, Nonlinear dynamics of MEMS arches under harmonic electrostatic actuation, J. Microelectromech. Syst. 19 (3) (2010) 647–656.

[44] L. Liao, P. Chao, C. Huang, C. Chiu, DC dynamic and static pull-in predictions and analysis for electrostatically actuated clamped circular micro-plates based on a continuous model, J. Micromech. Microeng. 20 (1) (2010) 025013, (15 pages).

[45] L. Banks-Sills, Y. Hikri, S. Krylov, V. Fourman, Y. Gerson, H.A. Bruck, Measurement of Poisson's ratio by means of a direct tension test on micron-sized specimens, Sensors Actuators A 169 (1) (2011) 98–114.

[46] D.I. Caruntu, M. Knecht, MEMS cantilever resonators under soft AC voltage of frequency near natural frequency, J. Dyn. Syst. Meas. Control 137 (2015) 041016, http://dx.doi.org/10.1115/1.4028887, (8 pages).

[47] D.I. Caruntu, K.N. Taylor, Bifurcation type change of AC electrostatically actuated MEMS resonators due to DC bias, Shock Vib. 2014 (1) (2014) 1–9, Article ID 214 542023.

[48] D.I. Caruntu, J.S. Beatriz, Quantum dynamics effects on amplitude–frequency response of superharmonic resonance of second-order of electrostatically actuated NEMS circular plates, in: I. Giorgio, L. Placidi, E. Barchiesi, B.E. Abali, H. Altenbach (Eds.), Theoretical Analyses, Computations, and Experiments of Multiscale Materials, Series: Advanced Structured Materials, Springer, Cham, 2022, pp. 69–104, http://dx.doi.org/10.1007/978-3-031-04548-6, Chapter 4.

[49] M.I. Ibrahim, M.I. Younis, The dynamic response of electrostatically driven resonators under mechanical shock, J. Micromech. Microeng. 20 (1) (2010) 025006, (9 pages).

[50] M. Lakrad, M. Belhaq, Suppression of pull-in in a microstructure actuated by mechanical shocks and electrostatic forces, Int. J. Non-Linear Mech. 46 (2) (2011) 407–414.

[51] D.I. Caruntu, M. Botello, C.A. Reyes, J. Beatriz, Voltage response of superharmonic resonance of second order of electrostatically actuated MEMS cantilever resonators, J. Comput. Nonlinear Dyn. 14 (2019) 031005, http://dx.doi.org/10.1115/1.4042017, (8pp).

[52] D.I. Caruntu, M. Botello, C.A. Reyes, J. Beatriz, Frequency-amplitude response of superharmonic resonance of second order of electrostatically actuated MEMS resonators, Int. J. Non-Linear Mech. 133 (2021) 10371, http://dx.doi.org/10.1016/j.ijnonlinmec.2021.103719, (9 pages).

[53] D.I. Caruntu, Dynamic modal characteristics of transverse vibrations of cantilevers of parabolic thickness, Mech. Res. Commun. 36 (3) (2009) 391–404.

[54] D.I. Caruntu, Classical Jacobi polynomials, closed-form solutions for transverse vibrations, J. Sound Vib. 306 (3–5) (2007) 467–494.

[55] D.I. Caruntu, Factorization of self-adjoint ordinary differential equations, Appl. Math. Comput. 219 (14) (2013) 7622–7631.

[56] D.I. Caruntu, C.A. Reyes, Casimir effect on amplitude–frequency response of parametric resonance of electrostatically actuated NEMS cantilever resonators, in: B. Abali, I. Giorgio (Eds.), Developments and Novel Approaches in Biomechanics and Metamaterials, in: Advanced Structured Materials, vol. 132, Springer, Cham, 2020, http://dx.doi.org/10.1007/978-3-030-50464-9_15.